International Journal of Refrigeration 126 (2021) 210–221

Contents lists available at ScienceDirect

International Journal of Refrigeration

journal homepage: www.elsevier.com/locate/ijrefrig

Performance enhancement of adsorption cooling cycle by pyrolysis of Maxsorb III activated carbon with ammonium carbonate

Mohamed Ghazy[a], Ahmed Askalany[a], Ali Kamel[a], Kamal M.S. Khalil[b], Ramy H. Mohammed[c], Bidyut Baran Saha[d,e,*]

[a] Mechanical Engineering Department, Faculty of Technology and Education, Sohag University, Sohag 82524, Egypt
[b] Chemistry Department, Faculty of Science, Sohag University, Sohag 82524, Egypt
[c] Department of Mechanical Power Engineering, Zagazig University, Zagazig 44519, Egypt.
[d] International Institute for Carbon-Neutral Energy Research (WPI-I2CNER), Kyushu University, 744 Motooka, Nishi-ku, Fukuoka-shi, Fukuoka 819-0395, Japan
[e] Mechanical Engineering Department, Kyushu University, 744 Motooka, Nishi-ku, Fukuoka-shi, Fukuoka 819-0395, Japan

ARTICLE INFO

Article history:
Received 30 September 2020
Revised 29 December 2020
Accepted 29 December 2020
Available online 31 December 2020

Keywords:
Adsorption isotherm
Adsorption kinetics
COP
Maxsorb III
SCP

ABSTRACT

Maxsorb III is the best available microporous activated carbon. The parent Maxsorb III has been modified by pyrolysis in the presence of ammonia carbonate. The adsorption isotherms and kinetics of HFC404A onto the modified Maxsorb III are experimentally measured over 25 °C to 75 °C. Tóth and Dubinin-Astakhov models are utilized to fit the experimentally measured data. The isosteric heat of adsorption is calculated by applying the Clausius-Clapeyron equation. The adsorption kinetics of the modified Maxsorb III/HFC404A are fitted using the linear driving force model and Fickian Diffusion equation. Experimental measurements indicate that the modified Maxsorb III has a maximum uptake of 2.65 kg.kg^{-1} of HFC404A at 25 °C, which is the highest reached value till today.

Additionally, the adsorption cooling system efficacy is evaluated under typical operating conditions using the modified Maxsorb III/HFC404A pair. The modified Maxsorb III/HFC404A could achieve a specific cooling power (SCP) of 747 W per kg of adsorbent along with a coefficient of performance (COP) of 0.40. Compared to the parent Maxsorb III/HFC404A pair, the pyrolyzed Maxsorb III/HFC404A pair provides the SCP and COP by a factor of 2.23 and 1.7, respectively, which are are the current benchmark.

Amélioration des performances du cycle de refroidissement par adsorption par la pyrolyse du charbon actif Maxsorb III avec du carbonate d'ammonium

Mots clés: Isotherme d'adsorption; Cinétique d'adsorption; COP; Maxsorb III; Puissance de refroidissement spécifique

1. Introduction

The global ambition of sustainable development is hampered by rapid socio-economic development and continuous population growth. This has resulted in a substantial escalation of demand in energy consumption produced mainly using fossil fuels. This puts the world on the brink of an additional pollution crisis as energy, and environmental sectors are interconnected. In response to these linked troubles, there is a continuous demand to raise the contribution of renewable energy sources in the power generation mix. Adsorption technology is considered an outstanding candidate for cooling, refrigeration, and energy storage. It can address the energy-environment nexus in an efficient and effective way because it could be run by solar, geothermal heat, or even low-grade heat sources. It does not include moving parts like pumps or compressors. However, this technology is still under the technology readiness level and suffers from low performance in terms of

* Corresponding author at: International Institute for Carbon-Neutral Energy Research (WPI-I2CNER), Kyushu University, 744 Motooka, Nishi-ku, Fukuoka-shi, Fukuoka 819-0395, Japan.
E-mail address: saha.baran.bidyut.213@m.kyushu-u.ac.jp (B.B. Saha).

https://doi.org/10.1016/j.ijrefrig.2020.12.036
0140-7007/

Nomenclature

Nomenclature

C	Concentration, $kg.kg^{-1}$
C_o	Maximum concentration, $kg.kg^{-1}$
W_o	Maximum concentration, $cm^3.kg^{-1}$
COP	Coefficient of performance
C_P	Specific heat, $J.kg^{-1}\ K^{-1}$
D_s	Surface diffusivity, $m^{2}.s^{-1}$
D_{so}	Pre-exponential coefficient, $m^{2}.s^{-1}$
E_a	Activation energy, J/mol.
F_o	Factor
h_{fg}	Latent heat of vaporization, $J.kg^{-1}$
H_{st}	Heat of adsorption, $J.mol^{-1}$
$\dot{m}$	Mass flow rate, $kg.s^{-1}$
n	Measurement number/exponent
P	Pressure, Pa
R	Universal gas constant, $J.mol^{-1}\ K^{-1}$
R_g	Gas constant, $J.kg^{-1}\ K^{-1}$
R_p	Particle radius, m
SCE	Specific cooling energy, $kJ.kg^{-1}$
SCP	Specific cooling power, $W.kg^{-1}$
T	Temperature, K
t	Time, s/exponent
U	Overall heat transfer coefficienct, $W.m^{-2}.K^{-1}$
V	Volume, m^3
v	Specific volume, $m^3.kg^{-1}$

Greek symbols

α	Thermal expansion coefficient, K^{-1}

Subscripts

a	adsorbed
al	aluminum
ch	chilled
co	condenser
cu	copper
cw	cooling water
ev	evaporator
g	gas
hw	hot water
i	initial
ir	iron
in	inlet
p	particle
s	saturation/solid
sg	silica gel

Abbreviations

AC	activated carbon/adsorption cooling
ACF	activated carbon fiber
FD	Fickian diffusion
LDF	linear driving force
MOF	metal-organic frameworks
ODP	ozone depletion potential
TGA	Thermo-gravimetric analyzer

specific cooling power (SCP) and coefficient of performance (COP) due to challenges at the component and system level.

Adsorption cooling (AC) cycle performance is centered around the working pair (i.e., adsorbent material and refrigerant) used in the cycle. The specific cooling power (SCP) and coefficient of performance (COP) of AC cycle depend mainly on the capacity of the adsorbent and its adsorption rate and the latent heat of vaporization of the refrigerant. An adsorbent having a considerable internal surface area per unit mass is favored for having a higher adsorption capacity. The adsorption equilibrium uptake depends on the vapor pressure and adsorbent temperature. This relation is the adsorption isotherm, which is obtained via a volumetric technique and fitted using several models such as Langmuir, Dubinin–Astakhov (D–A), modified D–A, and Tóth model (Mohammed et al., 2018c). Therefore, measuring the adsorption isotherm of the adsorption working pair is a fundamental parameter in evaluating the SCP and COP of AC cycle. Hence, research efforts are focused on proposing new adsorbent materials with high adsorption capacity and high adsorption rate. Many physical adsorption working pairs have been proposed, and their adsorption isotherms have evaluated, such as activated carbon (AC)/methanol (Gordeeva and Aristov, 2014; Lu, 2019), AC/ethanol (Ismail et al., 2013; El-Sharkawy et al., 2015), Maxsorb III/ethanol (Bouzid et al., 2017; Thu et al., 2019), Maxsorb III/methanol (Thu et al., 2014; Baran et al., 2008), silica gel/water (Freni et al., 2019; Mohammed et al., 2018c), zeolite/water (Bellat et al., 2019; Chan et al., 2018), and MOFs/water (Furukawa et al., 2013; Han and Chakraborty, 2019).

Carbon and its derivatives are suitable adsorbents for adsorption cooling applications (Rupa et al., 2020). In this regard, Jribi et al. (Jribi et al., 2014) applied the linear driving force (LDF) model to simulate the effectiveness of the adsorption cycle using Maxsorb III/CO_2 as a working pair. It was highlighted that the cycle could deliver 25 $W.kg^{-1}$ of SCP with 0.1 COP value. Dakkama et al. (Dakkama et al., 2017) found that the adsorption cycle using a combination of Maxsorb/R134a and Maxsorb/propane working pair could produce a cooling power of 1.82 kW and a COP of 0.08. Sur et al. (2020) investigated the solar-driven adsorption cycle using activated carbon (AC)/methanol as a working fluid for milk storage application. The SCP of the system was about 5.4 $kW.kg^{-1}$. Thu et al. (2019) found that adsorption systems using Maxsorb III and ethanol can produce a cooling power from 15 W to 35 W depending on the adsorption time. Ghazy et al. (2020) presented that Maxsorb III/HFC404A can produce an SCP of 0.275 $kW.kg^{-1}$ and a COP of 0.23. These results are owing to the high maximum capacity of the Maxsorb III that was reported to be 2.2 $kg.kg^{-1}$ of HFC404A. Rupam et al. tested the performance of six different working pairs, namely, PR_KOH4/ethanol, SAC2/R32, Maxsorb III/ethanol, Maxsorb III/R152a, Maxsorb III/propane, and H_2-treatedMaxsorb III/ethanol. PR_KOH4/ethanol working pair has the highest value of cooling by 436.07 $kJ.kg^{-1}$ at a COP around 0.85.Shabir et al. (2020) reviewed the last recent research works on adsorption working pairs. This study concluded that Maxsorb III is a suitable adsorbent because of its high specific surface area.

Adsorption kinetics of working pairs is commonly predicted by either the Linear Driving Force (LDF) model or Fickian diffusion (FD) equation. Askalany and Saha (2015) showed that both FD and LDF could fit the experimental data of R32 in ACF-20 and Maxsorb III. The same agreement was presented for ACF/HFC410A using the LDF model (Askalany et al., 2014). Rupa et al. (2020) indicated that the LDF model is better than the FD model in tracking the instantaneous adsorption uptake of the activated carbon-graphene composite/ethanol pair. Jribi et al. (2017) presented equilibrium uptake and kinetics of Maxsorb III/CO_2. The maximum uptake was 1.3 $kg.kg^{-1}$ at 30°C. The modified LDF equation with a variable mass transfer parameter was used to fit the measured adsorption kinetics. Jribi et al. (2014) applied the LDF model to simulate the effectiveness of AC cycle using Maxsorb III/CO_2 as a working pair. It was highlighted that the cycle could result in 25 $W.kg^{-1}$ of SCP with 0.1 COP.

Besides the adsorption isotherm of the working pair, adsorption bed design is a key parameter affecting the kinetics of the AC cycle and hence its performance. Therefore, extensive research efforts have focused on enhancing the performance of adsorption tech-

nology by proposing new adsorbent materials and different bed designs. Hu et al. (2009) assessed the effectiveness of using zeolite/aluminum foam with water as a working pair for sorption cooling applications. The thermal conductivity of this material was measured to be 2.89 $W.m^{-1}$ $K^{-1,}$ which allowed the system to produce a cooling power of about 0.5 $kW.kg^{-1}$ at a COP of 0.5 using 77.5 °C desorption temperature. Lenzen et al. (2018) evaluated the performance of adsorption cooling unit using monolith of CAU-10-H/binder composite/water as a working pair. This system was able to deliver a cooling power of 1.369 $kW.kg^{-1}$. Mohammed et al. (2019a) packed silica gel into aluminum foam to enhance the overall thermal conductivity of a lab-scale adsorption bed. Results indicated that this bed arrangement could produce a specific cooling power (SCP) of 827 $W.kg^{-1}$ at a COP of 0.75. This remarkable improvement in the effectiveness is owing to the high adsorption rate due to the high thermal conductivity of silica gel/foam bed. Xu et al. (2020) prepared a composite of copper foam and MIL-101 (CFCM) using a dip-coating method and used it as an adsorption cooling bed. The thermal conductivity of this adsorbent was found to be 0.86 $W.m^{-1}.K^{-1}$. Compared with MIL-101, this value is 14 times higher and produced a cooling power of 4.442 $kW.m^{-3}$. Almohammadi and Harby (2020) performed optimization analyses for adsorption cooling cycle powered by solar energy. Results showed that the cycle could deliver an SCP of 0.145 $kW.kg^{-1}$ and a COP of 0.52 at the optimized conditions. Rezk et al. (2013) evaluated the performance of the adsorption cooling cycle using MIL-101Cr/Ethanol as a working pair. The ethanol adsorption uptake was measured to be 1.2 $kg.kg^{-1}$ of adsorbent. SCP of 0.126 $kW.kg^{-1}$ and COP of 0.18 were delivered from this system. (Xia et al. (2020) tested different adsorbents for cooling and heating applications. The tested applications were covalent-organic frameworks (COF-5), Cu-BTC, MIL-101(Cr), and ZIF-8, while water was used as adsorbate. The COF-5 exhibited a COP for heating and cooling of about 1.79 and 0.59, respectively.

The literature study points out that the performance of the adsorption system depends on the working pair. Among several candidates, Maxsorb III is found to be a potential adsorbent for the development of compact adsorption cooling cycle due to its huge surface area and it is affinity for Chlorofluorocarbons (CFC) and hydrochlorofluorocarbons (HCFC). Therefore, the primary target of the present study is to synthesize a modified version of Maxsorb III with a higher surface area, leading to a higher adsorption capacity. In this paper, Maxsorb III is pyrolyzed with an ammonia carbonate solution at 500°C to enhance its adsorption characteristics. HFC404A is a gaseous mixture proposed to replace R502 and R22 in low/medium temperature cooling applications. So, HFC404A is considered as an adsorbate (refrigerant) in the current work. Sorption features of the modified Maxsorb III/HFC404A are experimentally investigated. The D-A and Tóth models are applied to fit the measured sorption isotherm of the modified Maxsorb III/HFC404A. The adsorption kinetics of the produced material is studied using the LDF and FD models. The isosteric heat of adsorption is experimentally calculated. Besides, the performance of the adsorption cycle using the pyrolyzed Maxsorb III/HFC404A is investigated at typical operating conditions of an adsorption cooling cycle. A comparison between the cooling performance of the modified Maxsorb III and the parent Maxsorb III is also presented employing HFC404A as the refrigerant.

2. Experimental work

2.1. Synthesis of the modified Maxsorb III

The surface characteristics of activated carbon can be controlled either by physical or chemical activation (Salas-Enríquez et al., 2016). Chemical activation has many advantages over the other methods, such as the low energy and operating cost, higher carbon yields, and larger surface areas (Salas-Enríquez et al., 2016). Typically, chemical activation occurs at a high temperature in the presence of agents such as KOH, NaOH, Na_2CO_3, $AlCl_3$, $ZnCl_2$, and H_3PO_4 (Gañán-Gómez et al., 2006; Haykiri-Acma et al., 2006). In this study, Maxsorb III, as parent material, is activated by pyrolysis with ammonium carbonate ($(NH_4)_2CO_3$). The Maxsorb III sample is placed in a ceramic dish and mixed with the ammonium carbonate solution (5% wt. concentration) in a ratio of 7.5 g to 100 ml. The pyrolysis process is started when the sample is then placed in a Muffle furnace of 500 °C (ramp rate 10 °C/min) in the presence of N_2 gas with a flow rate of 150 $ml.min^{-1}$. After an hour, the temperature of the oven is gradually reduced, and the sample is taken out at room temperature. The modified activated carbon has been stirred and washed by HCl solution for 30 min, followed by filtration and washing with warm and cold distilled water. Finally, the resulted activated carbon material has been dried at 110 °C in a drying oven for 12 h. The sample is weighed before and after the chemical activation, so, the change in the sample mass could be estimated.

2.2. Experimental apparatus

Adsorption characteristics test-rig adopts the volumetric method to investigate isotherm and kinetic of adsorption pair. Fig. 1 presents a drawing of the components of the experimental device. The first step of the experiment is preparing the sample for measurement processes by evacuating the apparatus parts from water vapor at a vacuum pressure of 10^{-4} Pa with a regeneration sample at 100 °C for 6 h to extract any residual water vapor. In the evacuation process, all valves are opened, but the refrigeration cylinder is kept closed. Furthermore, the surrounding water temperature of the sample is fixed by a water circulator. Secondly, the vacuum valves V1 and V2 are shut down while V3 is kept open. The dosing tank is charged by HFC-404A at a certain pressure and then closed V3. Thirdly, when the pressure in the dosing tank reaches a steady-state condition, the valve of V2 opens until it reaches equilibrium pressure between the sample cell and the dosing tank and then closed V2. This procedure is repeated by increasing the charging pressure every time until saturation pressure to avoid a condensation state. The adsorption uptake can be measured at several surrounding temperatures varying from 25 °C to 75 °C.

Eqs. (1)–(4) shown below are used to estimate the adsorbed amount of the refrigerant at the adsorption temperature.

$$\Delta m_{load,n} = \left\{\rho_{ads,i}(P_i, T_{ads}) - \rho_{ads,f}\left(P_f, T_{ads}\right)\right\}_{load\ cell}(V_{load} + V_{tube}) \tag{1}$$

$$V_{void} = V_{ads} - \left(\frac{m_s}{\rho_s} + V_{pore}\right) \tag{2}$$

$$\Delta m_{void,n} = \left\{\rho_{ads,n}(P_i, T_{ads}) - \rho_{ads,n-1}\left(P_f, T_{ads}\right)\right\}_{ads\ cell}(V_{void}) \tag{3}$$

$$m_n = m_{n-1} + \Delta m_{load,n} - \Delta m_{void,\,n} \tag{4}$$

Where m is the adsorbed mass and n is the measurement number. The densities are extracted from REFPROP 9 as a function of temperature and pressure at constant volume for each cell and the connecting tubes. The micropore volume of adsorbent is considered to be constant.

2.3. Extraction of adsorption characteristics

2.3.1. Adsorption isotherms

Several theoretical models were suggested to track the experimental measurements of the adsorption equilibrium capacity of

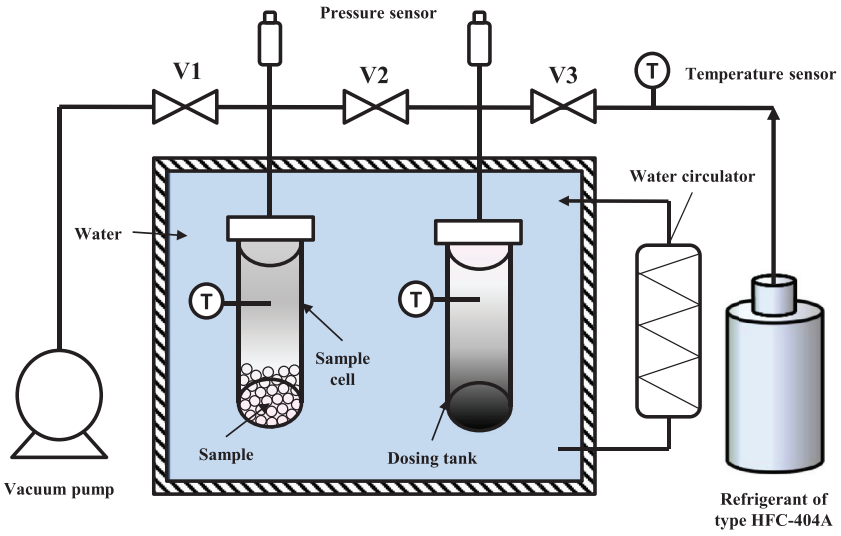

Fig. 1. A schematic of the experimental apparatus.

any working pair. Modified Dubinin–Astakhov (D–A) model and the Tóth model are usually utilized to track the measured adsorption uptake at different temperatures and pressures.

2.3.1.1. Modified Dubinin-Astakhov (D–A) model. This model is based on the theory of volume filling of micropores, which relies on the adsorbent temperature and refrigerant vapor pressure. D–A model can be expressed as (Mohammed et al., 2018c):

$$C = C_o \exp\left\{-\left(\frac{RT}{E}\ln\left(\frac{P_s}{P}\right)\right)^n\right\} \tag{5}$$

where C is the adsorption uptake at certain P *and* T (kg of refrigerant per kg of adsorbent material), C_o is the maximum uptake (kg of refrigerant per kg of adsorbent material), and P_s is the refrigerant vapor pressure at T.

2.3.1.2. Tóth model. The Tòth model is more suitable for monolayer and multilayer sorption (Tóth, 1995). The model can be written as (Mohammed et al., 2018c):

$$C = C_o \frac{bP}{\left\{1 + [bP]^t\right\}^{\frac{1}{t}}} \tag{6}$$

$$b = b_o \exp\left(\frac{H_{st}}{RT}\right) \tag{7}$$

where H_{st} is the isosteric heat of adsorption.

2.3.2. Isosteric heat of adsorption

The adsorption process is an exothermic reaction in which heat is generated and is called the isosteric heat of adsorption, which is an essential value for designing an efficient cooling unit. It is usually a function of relative pressure (P/P_s) or concentration, while it has a weak dependency on temperature. It can be given as (Ghazy et al., 2016):

$$H_{st} = \frac{P_s}{P}\frac{(v_g - v_a)}{(v_g - v_f)}h_{fg} + P(v_g - v_a)\ln\left(\frac{P_s}{P}\right)\left(\frac{\alpha T}{n\ln\left(\frac{W_o}{Cv_a}\right)}\right) \tag{8}$$

where α is the thermal expansion coefficient (K^{-1}) and h_{fg} is the latent heat of vaporization ($J.mol^{-1}$).

2.3.3. Adsorption kinetics

Accurate tracking of the instantaneous sorption uptake of the working pair directly affects the AC cycle performance. Adsorption uptake of the working pair as a function of time can be measured by many proposed models (Ruthven, 2008). The LDF model and FD model are used in this study.

The LDF model: The linear driving force (LDF) approximation describes the diffusion-controlled kinetics of vapor onto the adsorbent. It can be expressed as (Choi et al., 2001; Ruthven, 2008):

$$\frac{C - C_{in}}{C_o - C_{in}} = 1 - \exp\left(-k_s a_v (t - t_{in})\right) \tag{9}$$

$$k_s a_v = F_o \frac{D_s}{R_p^2} \tag{10}$$

where C_{in} is the initial concentration ($kg.kg^{-1}$), t_{in} is the initial time (s), R_p is the average radius of adsorbent particle (m), and D_s is the diffusivity of vapor into adsorbent ($m^2.s^{-1}$) which is given as (Askalany et al., 2014; Mohammed et al., 2018a):

$$D_s = D_{so}\exp\left(-\frac{E_a}{RT}\right) \rightarrow \ln(D_s) = \ln(D_{so}) - \frac{E_a}{RT} \tag{11}$$

where E_a is the activation energy ($J.mol^{-1}$) and D_{so} is the pre-exponential coefficient ($m^2.s^{-1}$). Both E_a and D_{so} can be extracted by plotting $\ln(D_s)$ versus 1/T. This relationship is called the Arrhenius curve where $\frac{E_a}{R}$ is the slope and D_{so} is the intercept.

The FD model: The FD equation is also usually employed to track the kinetics of different adsorption working pairs. The Fickian model is an unsteady 1-D diffusion equation. The algebraic form of the FD equation is valid when the diffusivity does not depend on concentration, and it is given as (Choi et al., 2001):

$$\frac{C}{C_o} = 1 - \frac{6}{\pi^2}\sum_{n=1}^{\infty}\frac{1}{n^2}\exp\left(-\frac{n^2\pi^2 D_s t}{R_p^2}\right) \tag{12}$$

3. Adsorption cooling cycle

The adsorption cooling cycle has a pair of adsorption/desorption beds, a condenser, and an evaporator (Askalany et al., 2017). The adsorption cooling cycle undergoes the heating-desorbing process and cooling-adsorbing process in which SCP is produced (Mohammed et al., 2018b). A mathematical lumped model, including the energy and mass balances of each component, has been used and validated by the same authors in their previous

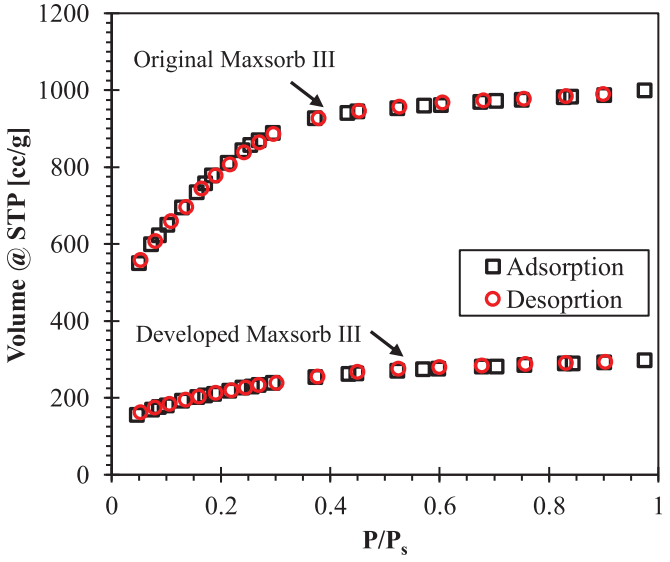

Fig. 2. N_2 gas adsorption by the original and developed Maxsorb III at 77 K.

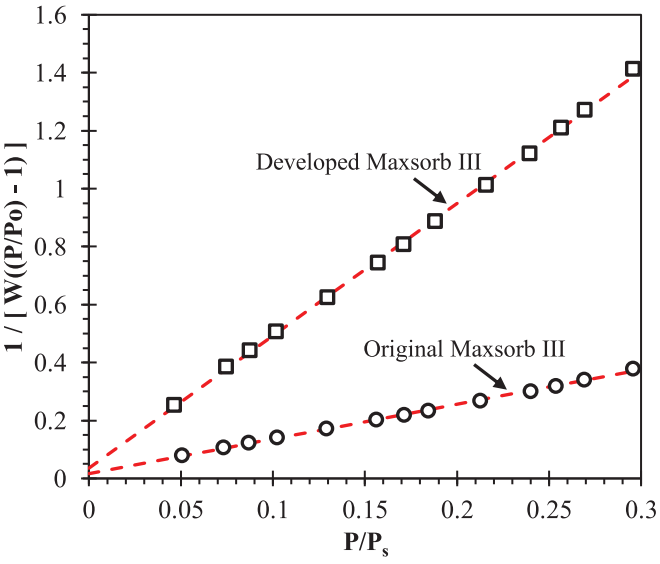

Fig. 3. BET plot of the original and developed Maxsorb III.

(Askalany et al., 2017; Mohammed et al., 2019b). The validated numerical model is used in this research work to assess the performance of the adsorption cooling cycle at different operating parameters using the modified Maxsorb III/HFC404A.

4. Results and discussion

The present section presents the experimental measurements of the adsorption characteristics of the modified Maxsorb III/HFC404A. The adsorption kinetics and adsorption isotherm are used to assess the effectiveness of the adsorption cooling cycle using a mathematical lumped parameter model.

4.1. Surface characterization analysis

Surface area, micropore volume, and pore size distribution of adsorbent are key parameters controlling the adsorption process. The surface area of the original and developed Maxsorb III is evaluated using N_2 gas adsorption at 77 K as given in Fig. 2. The surface area analysis is carried out by following the Brunauer-Emmett-Teller (BET) method with multi-points surface area analysis that is adopted and plotted in Fig. 3 for the developed Maxsorb III. It is observed that the developed Maxsorb III has a BET surface area of about 756.316 m^2/g, compared to 2873.61 m^2/g for the original Maxsorb III. So, the processes that have been done on the original material reduce the surface area significantly. Pore Size Distribution (PSD) is also fundamental information of the porous material. It is used to determine the population of pores as a function of the pore size. The pore-size distribution analyses are conducted using the Density Functional Theory (DFT) method. Fig. 4 shows the cumulated pore volume and PSD analysis of the original and developed Maxsorb III adsorbent. The pore volume distribution profile of both materials has a peak of around 1.3 nm half pore width. Interestingly, the developed Maxsorb III has other peaks in the micropore region and in the mesopores region. This pore size distribution directly affects the adsorption characteristics of the developed material. Thus, it is expected that the adsorption mechanism might change from surface coverage to pore filling because the pore sizes change from mesopores to micropores (Do, 1998).

The surface characteristic analysis of the developed Maxsorb III is summarized in Table 1 and compared with the original Maxsorb III. It can be seen that the surface area of the developed adsorbent is much less than that of the original one. This is attributed to the

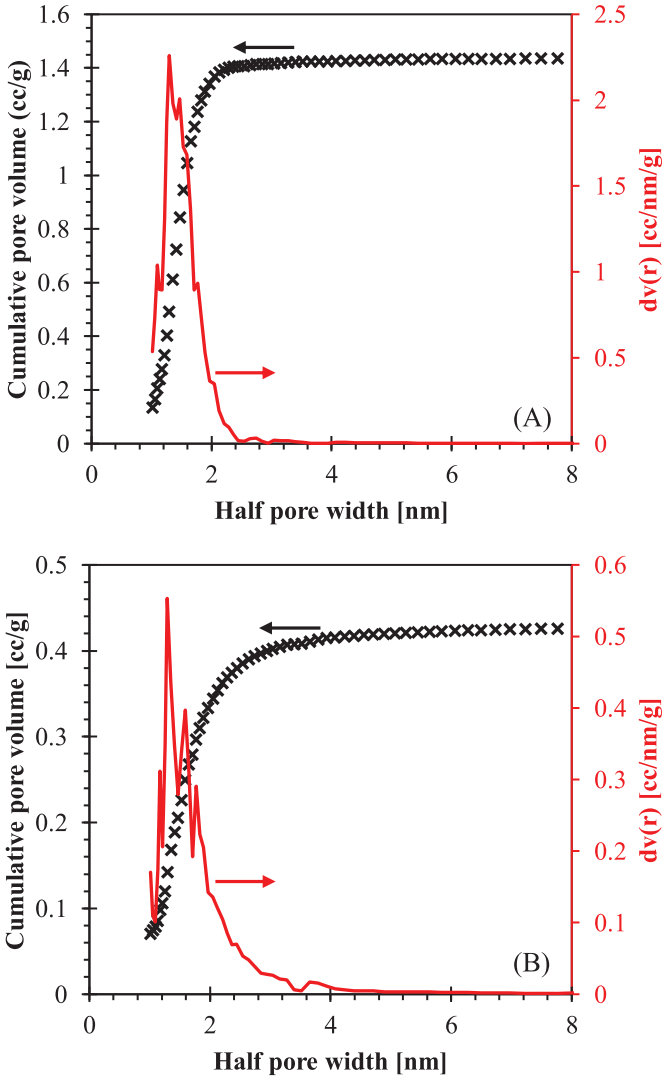

Fig. 4. PSD analysis of the (A) original Maxsorb III and (B) developed one using the DFT method.

Table 1
Surface characterization analysis of the developed Maxsorb III.

Parameter	Original Maxsorb III	Developed Maxsorb III
BET surface area (m^2/g)	2873.61	756.316
Total pore volume (cm^3/g)	1.55	0.459
Average pore diameter (nm)	2.16	2.4

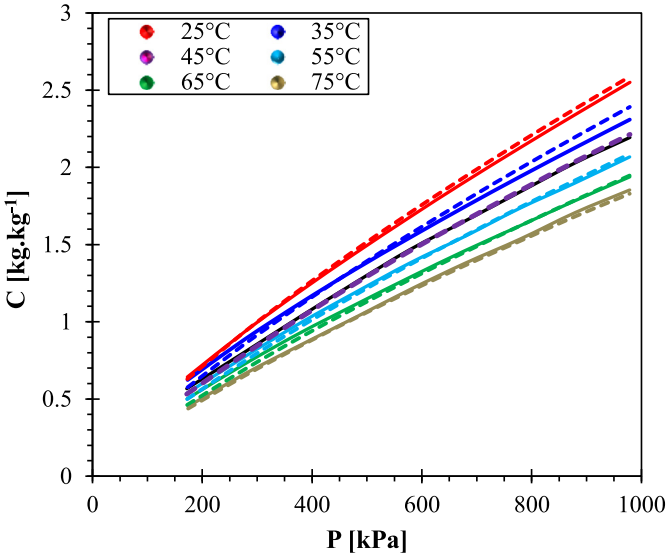

Fig. 5. Fitting the experimental adsorption data (symbols) of modified Maxsorb III/HFC404A using the Tóth (dashed lines) and D-A (solid lines) model.

fact that the pyrolysis process simultaneously changes the physical phase and chemical composition. This process directly affects the pore volume as well. The total pore volume is reduced from 1.545 cc/g to 0.459 cc/g. It is worth mentioning that the value of the measured BET surface area considers mainly the multilayer adsorption in mesopores.

4.2. Adsorption characteristics

The adsorption uptakes of HFC404A onto the modified Maxsorb III at several pressures and temperatures are found experimentally and plotted, as given in Fig. 5. The maximal sorption uptake of the modified Maxsorb III/HFC404A is found to be 2.65 $kg.kg^{-1}$. The adsorption uptake is found to increase linearly as the vapor pressure rises. The adsorption equilibrium uptake of the modified Maxsorb III raises as the adsorbent temperature decreases at the same pressure. The deviation between the curves increases as the pressure increases. At a vapor pressure of 980 kPa, the adsorption uptake at 25 °C is higher than that at 75 °C by a factor of 1.4. This trend reflects the high dependence of the equilibrium uptake of HFC404A onto the modified Maxsorb III on the temperature of the adsorbent. The experimental measurements are fitted by using the modified D–A model and the Tóth equation. Circles in Fig. 5 are symbolized for the experimental data. The solid lines are marks for the modified D-A model, while the dashed lines represent the Tóth model. It is clear that both the modified D-A model and the Tóth model fit the current experimental sorption isotherms. While the

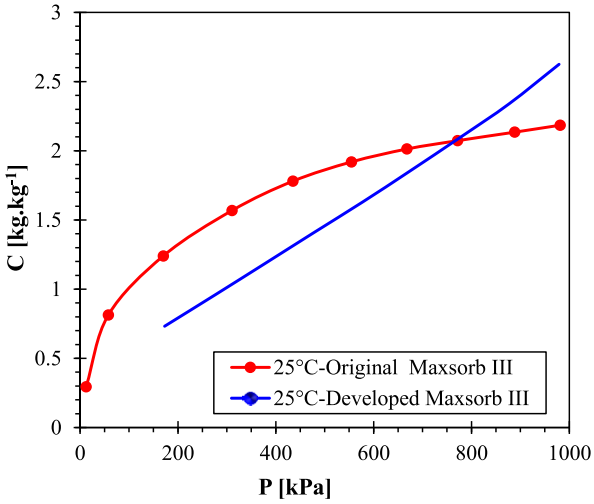

Fig. 6. Adsorption isotherm of the modified Maxsorb III against the parent Maxsorb III at 25 °C.

modified D–A model has the best agreement between the experimental results and predicted ones. Both adsorption isotherm models (i.e., LDF and FD) track the experimental measurements with a relative error of less than ±8% at the low relative pressure and less than ±6% at the high relative pressure. This small error also reflects the appropriateness of both models in fitting the experimental data with a little preference for the D-A model. Table 2 presents the fitting parameters and coefficients of the modified D-A model and the Tóth model (i.e., Eqs. 5, 6, and 7).

The adsorption characteristics of the original Maxsorb III/HFC404A is estimated by following the same procedure and the same experimental setup. The measured sorption isotherms of the modified Maxsorb III/HFC404A and the original Maxsorb III/HFC404A are compared, as plotted in Fig. 6. The adsorption isotherm of the original Maxsorb III/HFC404A follows Type I isotherm, while the modified Maxsorb III/HFC404A is characterized by linear behavior. This trend indicates that the adsorption of HFC404A on the developed Maxsorb III follows a mechanism of pore volume-filling rather than the surface coverage mechanism (formation of successive layers) as in the original Maxsorb III. In micropores, the mechanism is due to micropore filling because of the adsorption force field encompassing the entire volume of micropores (Schneider, 1995). Also, there is a probability of the presence of the functional group(s) due to the pyrolysis process that positively affects the adsorption isotherm of the developed Maxsorb III. This hypothesis will be investigated in detail in our future works.

The original Maxsorb III outperforms the modified one in terms of adsorption equilibrium at low pressure, which is out of the operating range of the adsorption cooling cycle. Interestingly, the maximum uptake of the modified Maxsorb III/HFC404A at 980 kPa is 2.65 $kg.kg^{-1}$ compared to 2.2 $kg.kg^{-1}$ for the original Maxsorb III/HFC404A. Additionally, Table 2 presents the maximum adsorption capacity for different versions of Maxsorb III. This figure indicates that the Maxsorb III modified in this study has the highest maximum adsorption uptake. This trend illustrates that the modi-

Table 2
Coefficients of the D-A model and the Tóth model.

Parameter	W_n (cm^3/kg)	C_n (kg/kg)	E (kJ/kg)	b_n (kJ/kg)	n	t	H_{st} (kJ/kg)
D-A	4.21	–	4075.39	–	1.19	–	–
Tóth	–	2.35	–	3.83E−07	–	0.25	7381.25

Table 3
Maximum adsorption capacities for different adsorption working pairs, including the present one.

Working pair	Adsorption uptake ($kg.kg^{-1}$)	Reference
KOH-H_2 treated Maxsorb III/ethanol	1.0	(El-Sharkawy et al., 2014)
(90% activated carbon +10% graphene)/ethanol	1.08	(Pal et al., 2019)
Maxsorb III/methanol	1.1	(El-Sharkawy et al., 2009)
H_2 treated Maxsorb III/ethanol	1.23	(El-Sharkawy et al., 2008)
Maxsorb III/R507A	1.3	(Habib et al., 2010)
Maxsorb III/CO_2	1.57	(Jribi et al., 2017)
Maxsorb III/HFC410A	1.8	(Askalany et al., 2014)
Maxsorb III/HFC134a	2.0	(Saha et al., 2009)
Original Maxsorb III/HFC404A	2.22	The present study
Developed Maxsorb III/HFC404A	2.65	The present study

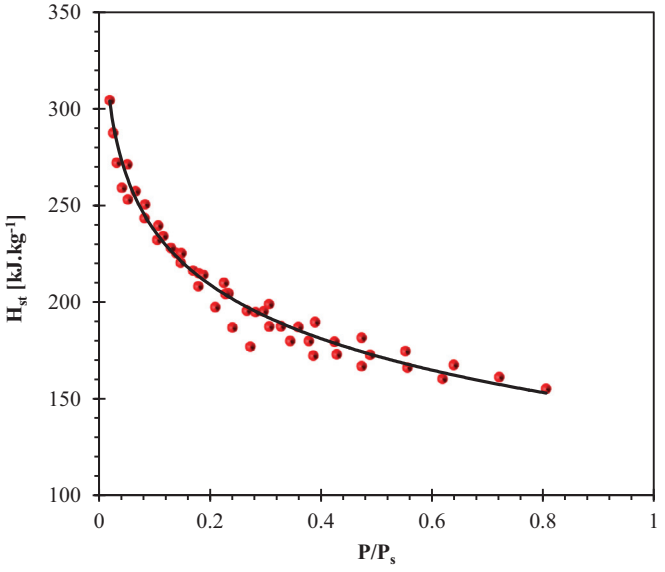

Fig. 7. Isosteric heat of adsorption against the relative pressures for the modified Maxsorb III/HFC404A.

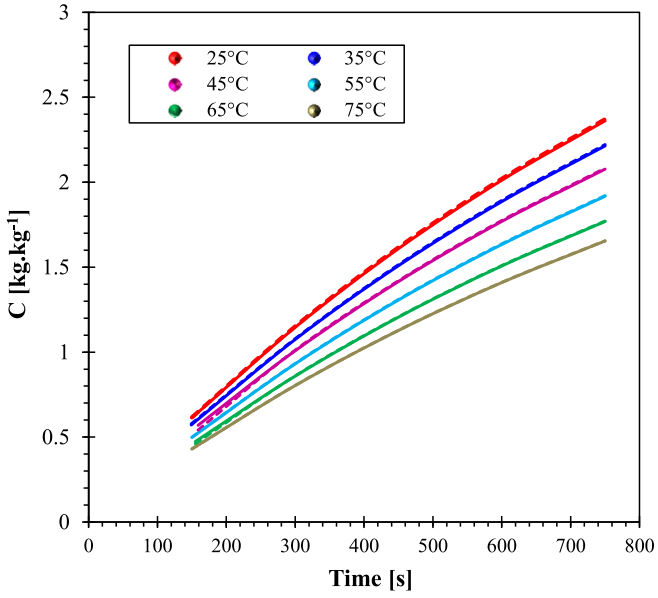

Fig. 8. LDF (solid lines) and FD (dashed lines) model versus experimental sorption kinetics of the modified Maxsorb III/HFC404A at different adsorption temperatures.

fied Maxsorb III could produce more SCP and COP than the other adsorption working pairs.

Fig. 7 shows the isosteric heat of adsorption extracted from the measurements at various relative pressures for the modified Maxsorb III/HFC404A. The heat of adsorption decreases exponentially as the relative pressure increases. When HFC404A molecules are exposed to the adsorbent, it first begins to fill up the narrow pore sizes with a sharp reaction producing high adsorption heat. Then this heat gradually decreases as the size of adsorbed pores increases. The figure points out that the heat of adsorption becomes higher when the adsorbent temperature drops. A logarithmic relationship (i.e., Eq. 13) between the isosteric heat of adsorption and relative pressure is identified by fitting the measured data as follows:

$$H_{st} = -40.26 \ln\left(\frac{P}{P_s}\right) + 144.23 \ \left(kJ.kg^{-1}\right) \quad (13)$$

The adsorption kinetics of the modified Maxsorb III/HFC404A is measured experimentally at different adsorption temperature, and the data is fitted using the LDF and FD models as plotted in Fig. 8. A proper matching among the experimental data and the predicted ones using the LDF and FD models are established, with a relative error less than ±8%. This trend reflects the appropriateness of both models in the accurate tracking of the instantaneous adsorption uptake of the modified Maxsorb III/HFC404A. The measured surface diffusivity is fitted using a linear equation to extract the D_{so} *and* E_a. The E_a and D_{so} for the modified Maxsorb III/HFC404A are calculated to be 82.16 $kJ.mol^{-1}$ and 2.84×10^{-14} $m^2.s^{-1}$, respectively.

4.3. Adsorption cooling cycle performance

In this section, the performance of the adsorption cooling cycle using the modified Maxsorb III/HFC404A as a working pair is evaluated. The adsorption cooling (AC) cycle considered for this study is the basic one that has two adsorption beds, a condenser, and an evaporator (Ahmed S. Alsaman et al., 2017; Askalany et al., 2020). Fig. 9 shows the basic AC system on the P-T-C diagram. The lumped parameter model is applied to calculate the temporal variation of the adsorption beds temperature and uptake at various operating conditions.

The employed model has been validated in many previous works done by the authors, such as in Refs. (Ali et al., 2020; Ahmed S Alsaman et al., 2017; Askalany et al., 2020, 2017; Mohammed et al., 2019b) at the operating conditions and design parameters are shown in Table 4. Fig. 7 presents the temporal temperature variations of adsorption beds, condenser, evaporator, cooling, and heating water. The operating parameters of the adsorption cooling unit shown in the P-T-C diagram are 95 °C hot water inlet temperature, 5 °C chilled water temperature, and 25 °C cooling water inlet temperature for the condenser. The cycle time is selected to be 450 s. The measured adsorption isotherm and adsorption kinetics of the modified Maxsorb III/HFC404A are used in the

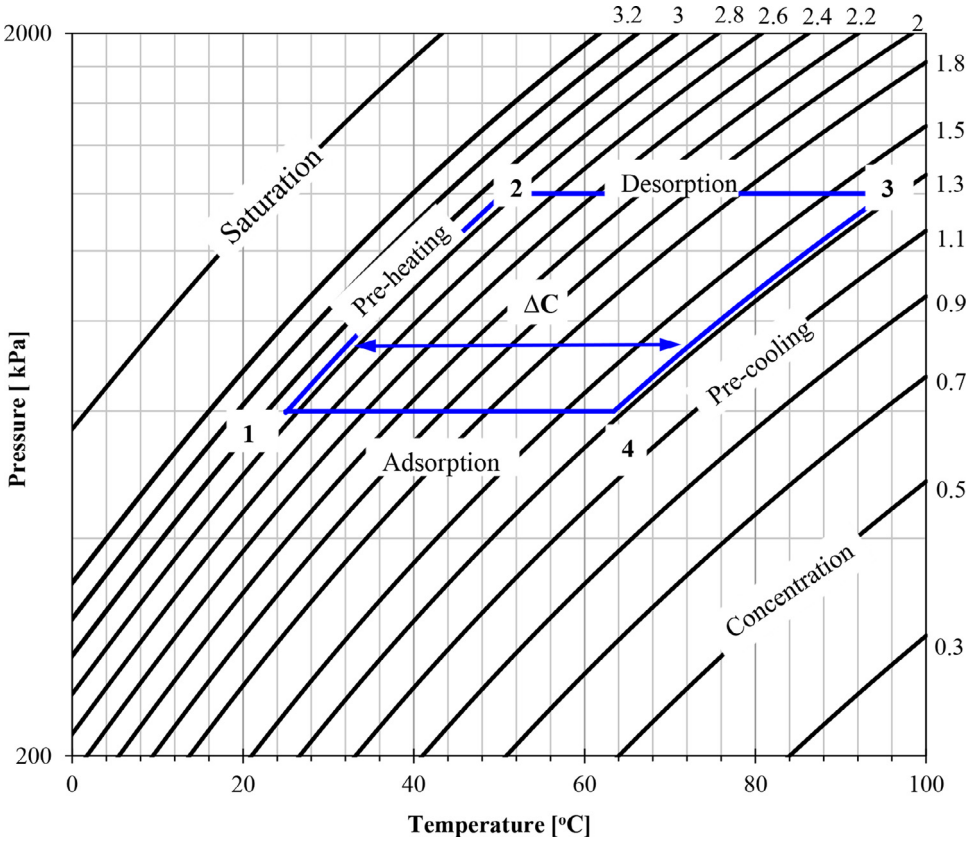

Fig. 9. Representation of the adsorption cooling processes on the P-T-C diagram using the modified Maxsorb III/HFC404A.

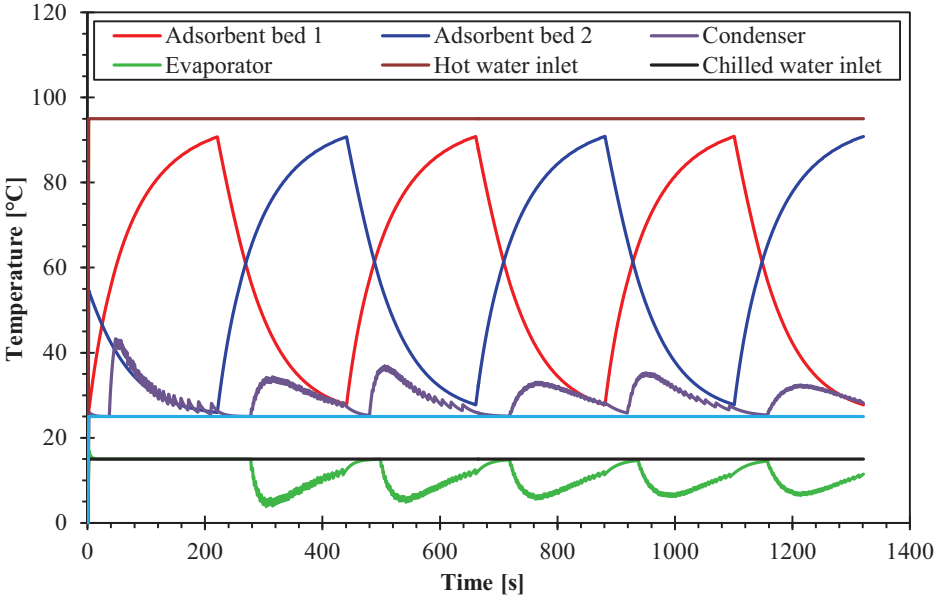

Fig. 10. Dynamic thermal behavior of each component in the adsorption cycle.

lumped parameter model to estimate the temporal variation of the instantaneous uptake of HFC404A onto the modified Maxsorb III, as presented in Fig. 10. The adsorption uptake change is found to be around 1.035 kg.kg^{-1} through the adsorption process, as shown in Fig. 11.

Fig. 12 presents the SCP and COP of a 2-bed adsorption cooling cycle using the original Maxsorb III and the modified one in this study at different half-cycle times. Results reveal that the SCP and COP provided using the modified Maxsorb III/HFC404A is much more than that produced using the original Maxsorb III/HFC404A. The optimal half-cycle time is found to be around 220 s. Beyond the optimal cycle time, the SCP steadily decreases. At the optimal cycle time, the SCP of the modified Maxsorb III/HFC404A is 2.2 times higher than that produced by the parent one. The COP of both working pairs enhances for longer half-cycle times. The COP provided by the modified Maxsorb III/HFC404A is always more

Table 4
The main operating conditions and design parameters used in the present study.

Parameter	Value	Unit
UA_{bed}	600	W/K
UA_{co}	500	W/K
UA_{ev}	350	W/K
M_{cu}	2.97	kg
M_{al}	0.72	kg
M_{ir}	15	kg
M_{sg}	6.75	kg
$\dot{m}_{ch}$	0.055	kg/s
$\dot{m}_{hw}$	0.2	kg/s
$\dot{m}_{cw}$	0.3	kg/s
$T_{ch,in}$	25	°C
$T_{sw,in}$	25	°C
T_{co}	25	°C
n	2	–
t_{cycle}	900	s

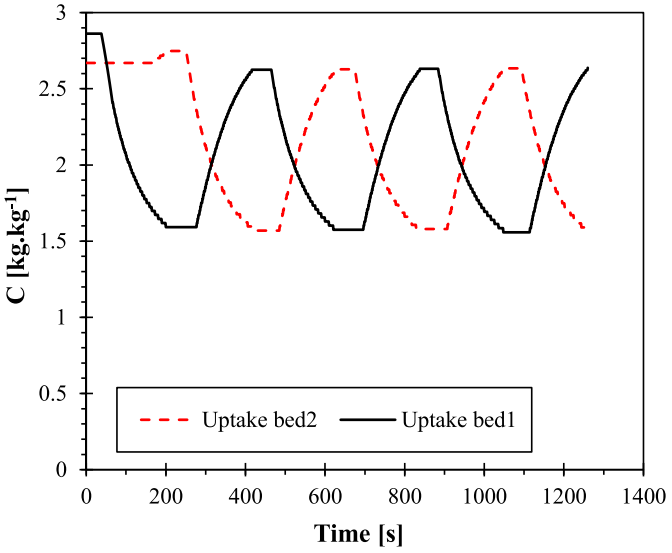

Fig. 11. Temporal behavior of bed uptake through the adsorption and desorption periods.

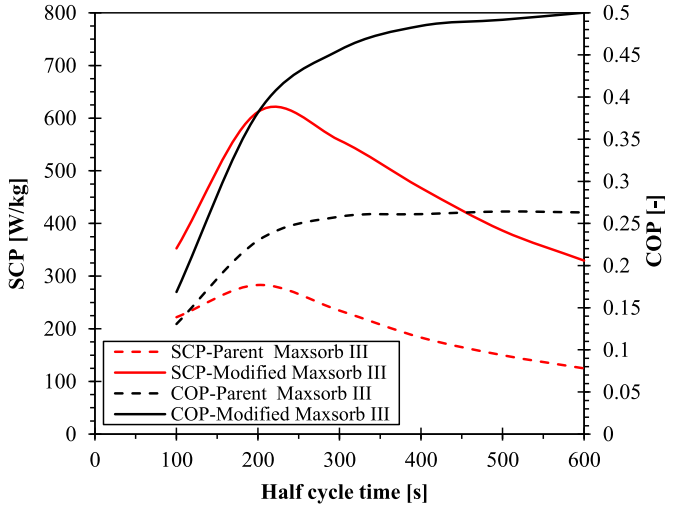

Fig. 12. SCP and COP with time at a cooling temperature of 25 °C and a heating temperature of 85 °C.

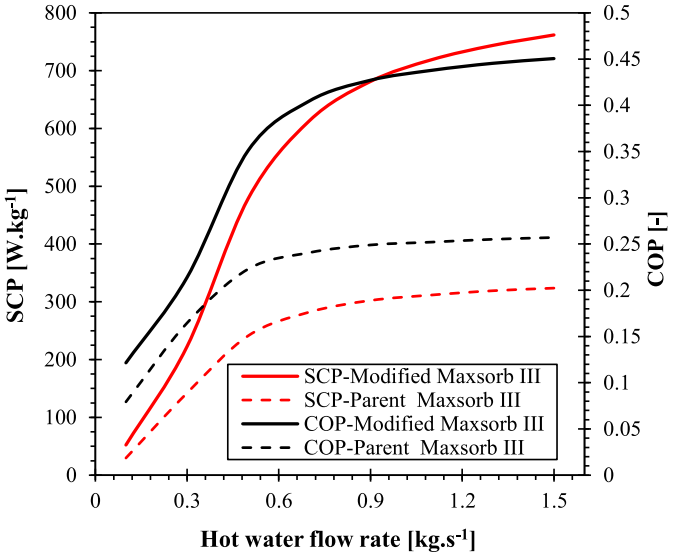

Fig. 13. Impact of the hot water flow rate on SCP and COP of the adsorption cooling cycle using the modified Maxsorb III/HFC404A.

than that of the original pair regardless of the cycle time. At 600 s half-cycle time, the COP increases by a factor of 2.0 using the modified Maxsorb III/HFC404A. Therefore, it can be concluded that using the modified Maxsorb III/HFC404A has a significant positive effect on the adsorption cooling cycle performance.

For further investigation of the adsorption cooling cycle employing the modified Maxsorb III/HFC404A, the impact of the flow rate of the hot fluid on the cycle performance is presented in Fig. 13. Increasing the hot water flow rate from 0.1 to 0.7 kg.s^{-1} makes a considerable enhancement in the SCP, and the COP of the adsorption cooling system employed the modified Maxsorb III. The trend of SCP and COP level off at 0.7 kg.s^{-1} mass flow rate. These results reveal the significant influence of the amount of hot water on the adsorption cooling cycle performance. Using 1.5 kg.s^{-1}, the modified Maxsorb III/HFC404A produces an SCP of 762 W.kg^{-1} at 0.45 COP. In turn, the parent Maxsorb III/HFC404A could deliver only an SCP of 324 W.kg^{-1} at 0.257 COP. Therefore, the SCP and COP increase by a factor of 2.35 and 1.75, respectively, using the modified Maxsorb III/HFC404A.

Table 5
Performance of the developed Maxsorb III/HFC404A adsorption system compared to previous research works.

Working pair	SCP (W.kg^{-1})	COP (-)	Reference
Maxsorb III/CO_2	25	0.1	(Jribi et al., 2014)
Maxsorb III/HFC134a	87	0.33	(Askalany et al., 2013)
Maxsorb III/methanol	90.39	0.75	(El-Sharkawy et al., 2009)
Maxsorb III/HFC32	200	0.18	(Askalany and Saha, 2015)
Maxsorb III/ethanol	228	0.68	(El-Sharkawy et al., 2008)
Original Maxsorb III/HFFC404A	275	0.24	The present study
Developed Maxsorb III/HFC404A	610	0.4	The present study

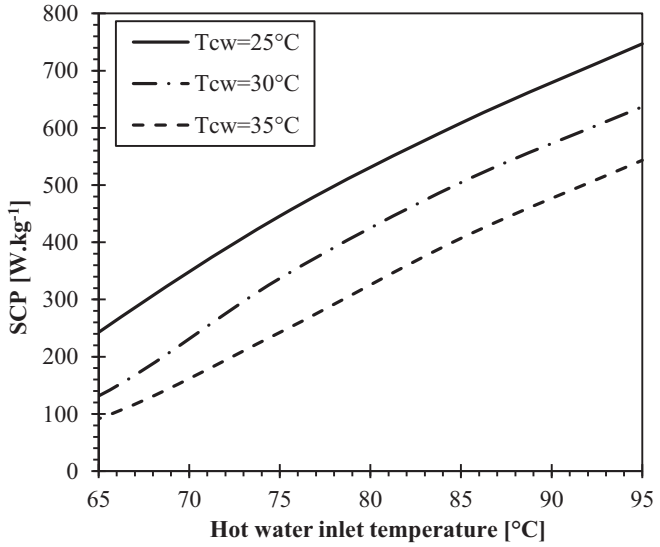

Fig. 14. Effect of the hot water inlet temperature on SCP of the adsorption cooling cycle using the modified Maxsorb III/HFC404A at different cooling temperatures.

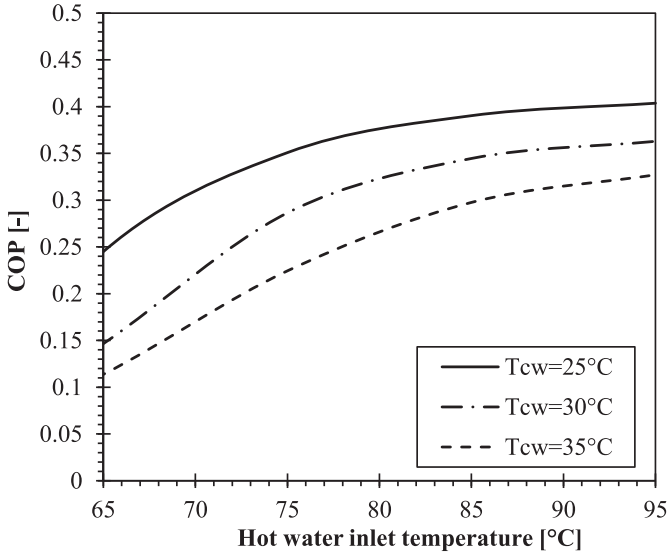

Fig. 15. Hot water inlet temperature effect on COP of the adsorption cooling cycle using the modified Maxsorb III/HFC404A at different cooling temperatures.

Fig. 14 depicts the influence of the hot water temperature on the produced SCP via the modified Maxsorb III/HFC404A using different cooling water temperatures. Results indicate that the adsorption cooling system can be run using low-grade heat of 60 °C. The SCP of the modified Maxsorb III/HFC404A system increases monotonically when the regeneration temperature rises. Also, the SCP enhances as the cooling water temperature decreases owing to the more increase in the uptake change through the adsorption period. Analysis of results highlights that the SCP enhances by a factor of 54.0 when the hot water temperature changes from 55 °C to 95 °C (747 W.kg^{-1} compared to 13.786 W.kg^{-1}). At a hot water inlet temperature of 95 °C, the delivered SCP is 747 W.kg^{-1} and 461 W.kg^{-1} using a cooling water temperature of 25 °C and 40 °C, respectively. Similarly, the influence of the inlet temperature of hot water on the COP of the modified Maxsorb III/HFC404A AC system at various inlet temperatures of cooling water is plotted in Fig. 15. The COP rises as the desorption temperature increases, and cooling water temperature decreases. The increase in the COP is steeper when the heating water temperature increases from 55 °C

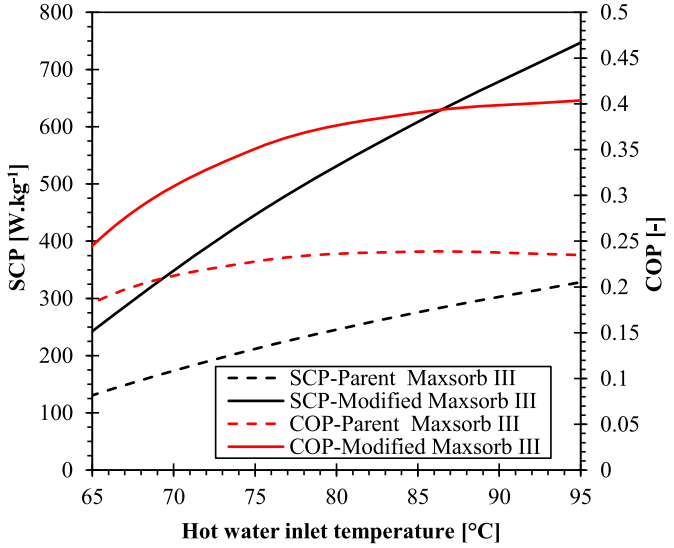

Fig. 16. Comparison between SCP and COP produced using the modified Maxsorb III and the original one.

to 80 °C. Using 0.7 kg/s mass flow rate of hot water, the maximum COP of 0.4 is achieved using 95 °C heating water temperature and 25 °C cooling water temperature, similar to the maximum SCP.

The performance of the modified Maxsorb III/HFC404A AC system and the parent one is compared at different hot water inlet temperatures, as plotted in Fig. 16. Generally, the SCP and COP of the modified Maxsorb III/HFC404A system are much higher than that of the original Maxsorb III/HFC404A when heating water temperature more than 60 °C is used. The enhancement in the adsorption cooling cycle performance increases when the heating water temperature rises. Using 95 °C heating water temperature, SCP produced by the modified Maxsorb III/HFC404A AC system is found to be 747 W.kg^{-1} compared to 328 W.kg^{-1} using the original Maxsorb III/HFC404A. The COP of the modified Maxsorb III/HFC404A AC system is calculated as 0.4 at 95 °C hot water inlet temperature, compared to 0.234 using the original Maxsorb III/HFC404A. Compared to the original Maxsorb III/HFC404A, the modified Maxsorb III/HFC404A increases the adsorption uptake, SCP, and COP by 20.50%,100.0%, and 123.0%, respectively.

Moreover, the performance of the modified Maxsorb III/HFC404A AC system investigated in this study is compared with the previous studies. Table 4 compares the performance of the adsorption cooling cycle using the modified Maxsorb III/HFC404A and other working pairs. At the same operating conditions, it is evident that the modified Maxsorb III/HFC404A outperforms the parent Maxsorb III with different refrigerants. The modified Maxsorb III/HFC404A could deliver an SCP of 610 W.kg^{-1} using a heating water temperature of 85 °C, which is much more than the best performance of Maxsorb III available in the open literature (Askalany and Saha, 2015; El-Sharkawy et al., 2009, 2008; Jribi et al., 2014) Therefore, the new version of Maxsorb III modified in this study is recommended for adsorption cooling applications.

5. Conclusions

In this paper, a highly porous Maxsorb III adsorbent is treated and modified by pyrolysis to enhance its adsorption characteristics. The adsorption equilibrium uptakes and adsorption kinetics of the modified Maxsorb III/HFC404A are studied experimentally by following the volumetric method. The experimental equilibrium uptakes are fitted correctly using the modified D–A equation, while

the adsorption kinetics is tracked accurately using either the LDF model or the FD model. The highest adsorption capacity of the modified Maxsorb III/HFC404A is higher than that of the original one by about 20.50% (2.65 kg.kg^{-1} compared to 2.22 kg.kg^{-1}). Such a relatively high value of adsorption capacity is the highest uptake comparing to the know activated carbon. A lumped parameter model using the experimental data is adopted to investigate the effectiveness of AC cycle using the modified Maxsorb III/HFC404A. It is found that the AC cycle using the modified Maxsorb III/HFC404A pair could be driven by low generation temperature. The numerical results point out that the performance of the modified Maxsorb III/HFC404A AC cycle is much better than that of the conventional one in terms of both SCP and COP. The modified Maxsorb III/HFC404A pair could result in an SCP of 747 W per kg of adsorbent at a COP of 0.4 using a 95 °C inlet temperature of hot water. The recorded SCP is the highest available value for the carbon-based adsorbents. Compared with different versions of Maxsorb III presented in the open literature, the modified one in this study has a higher SCP by a factor of 2.2 at the same operating conditions, which are the current benchmark. Due to the higher sorption equilibrium uptake of HFC404A onto the modified Maxsorb III and the low driving temperature (less than 100 °C), the proposed pair is recommended for adsorption cooling applications driven by low-grade heating sources or solar energy.

Declaration of Competing Interest

The authors declare that they have no known competing financial interests or personal relationships that could have appeared to influence the work reported in this paper.

References

Ali, E.S., Mohammed, R.H., Askalany, A., 2020. A daily freshwater production of 50 m^3/ton of silica gel using an adsorption-ejector combination powered by low-grade heat. J. Clean. Prod., 124494 doi:10.1016/j.jclepro.2020.124494.

Almohammadi, K.M., Harby, K., 2020. Operational conditions optimization of a proposed solar-powered adsorption cooling system: Experimental, modeling, and optimization algorithm techniques. Energy 206, 118007 https://doi.org/10.1016/j.energy.2020.118007.

Alsaman, Ahmed S., Askalany, A.A., Harby, K., Ahmed, M.S., 2017. Performance evaluation of a solar-driven adsorption desalination-cooling system. Energy doi:10.1016/j.energy.2017.04.010.

Askalany, A., Ali, E.S., Mohammed, R.H., 2020. A novel cycle for adsorption desalination system with two stages-ejector for higher water production and efficiency. Desalination 496, 114753. doi:10.1016/j.desal.2020.114753.

Askalany, A.A., Henninger, S.K., Ghazy, M., Saha, B.B., 2017. Effect of improving thermal conductivity of the adsorbent on performance of adsorption cooling system. Appl. Therm. Eng. 110, 695–702. doi:10.1016/j.applthermaleng.2016.08.075.

Askalany, A.A., Saha, B.B., 2015. Experimental and theoretical study of adsorption kinetics of Difluoromethane onto activated carbons. Int. J. Refrig. 49, 160–168. doi:10.1016/j.ijrefrig.2014.10.009.

Askalany, A.A., Saha, B.B., Ahmed, M.S., Ismail, I.M., 2013. Adsorption cooling system employing granular activated carbon-R134a pair for renewable energy applications. Int. J. Refrig. 36, 1037–1044. doi:10.1016/j.ijrefrig.2012.11.009.

Askalany, A.A., Saha, B.B., Ismail, I.M., 2014. Adsorption isotherms and kinetics of HFC410A onto activated carbons. Appl. Therm. Eng. 72, 237–243. doi:10.1016/j.applthermaleng.2014.04.075.

Baran, S.B., Kandadai, S., Anutosh, C., Khairul, H., Ibrahim, E.S.I., Shigeru, K., 2008. Adsorption characteristics of Maxsorb-III + methane systems by desorption experiments. In: ASME International Mechanical Engineering Congress and Exposition, Proceedings, pp. 415–419. doi:10.1115/IMECE2007-42941.

Bellat, J.P., Weber, G., Bezverkhyy, I., Lamonier, J.F., 2019. Selective adsorption of formaldehyde and water vapors in NaY and NaX zeolites. Microporous Mesoporous Mater. 288. doi:10.1016/j.micromeso.2019.109563.

Bouzid, M., Ben Torkia, Y., Wjihi, S., Ben Lamine, A., 2017. Kinetic adsorption modeling of ethanol molecules onto three types of activated carbons: Microscopic interpretation of adsorption and diffusion parameters. J. Mol. Liq. 242, 98–108. doi:10.1016/j.molliq.2017.06.066.

Chan, K.C., Tso, C.Y., Wu, C., Chao, C.Y.H., 2018. Enhancing the performance of a zeolite 13X/CaCl2–water adsorption cooling system by improving adsorber design and operation sequence. Energy Build. 158, 1368–1378. doi:10.1016/j.enbuild.2017.11.040.

Choi, J.G., Do, D.D., Do, H.D., 2001. Surface diffusion of adsorbed molecules in porous media: monolayer, multilayer, and capillary condensation regimes. Ind. Eng. Chem. Res. 40, 4005–4031. doi:10.1021/ie010195z.

Dakkama, H.J., Elsayed, A., AL-Dadah, R.K., Mahmoud, S.M., Youssef, P., 2017. Integrated evaporator–condenser cascaded adsorption system for low temperature cooling using different working pairs. Appl. Energy 185, 2117–2126. doi:10.1016/j.apenergy.2016.01.132.

El-Sharkawy, I.I., Hassan, M., Saha, B.B., Koyama, S., Nasr, M.M., 2009. Study on adsorption of methanol onto carbon based adsorbents. Int. J. Refrig. 32, 1579–1586. doi:10.1016/j.ijrefrig.2009.06.011.

El-Sharkawy, I.I., Saha, B.B., Koyama, S., He, J., Ng, K.C., Yap, C., 2008. Experimental investigation on activated carbon-ethanol pair for solar powered adsorption cooling applications. Int. J. Refrig. 31, 1407–1413. doi:10.1016/j.ijrefrig.2008.03.012.

El-Sharkawy, I.I., Uddin, K., Miyazaki, T., Baran Saha, B., Koyama, S., Kil, H.S., Yoon, S.H., Miyawaki, J., 2015. Adsorption of ethanol onto phenol resin based adsorbents for developing next generation cooling systems. Int. J. Heat Mass Transf. 81, 171–178. doi:10.1016/j.ijheatmasstransfer.2014.10.012.

El-Sharkawy, I.I., Uddin, K., Miyazaki, T., Saha, B.B., Koyama, S., Miyawaki, J., Yoon, S.H., 2014. Adsorption of ethanol onto parent and surface treated activated carbon powders. Int. J. Heat Mass Transf. 73, 445–455. doi:10.1016/j.ijheatmasstransfer.2014.02.046.

Freni, A., Calabrese, L., Malara, A., Frontera, P., Bonaccorsi, L., 2019. Silica gel microfibres by electrospinning for adsorption chillers. Energy 187. doi:10.1016/j.energy.2019.115971.

Furukawa, H., Cordova, K.E., O'Keeffe, M., Yaghi, O.M., 2013. The chemistry and applications of metal-organic frameworks. Science doi:10.1126/science.1230444, (80-.).

Gañán-Gómez, J., Macías-García, A., Díaz-Díez, M.A., González-García, C., Sabio-Rey, E., 2006. Preparation and characterization of activated carbons from impregnation pitch by ZnCl 2. Appl. Surf. Sci. 252, 5976–5979. doi:10.1016/j.apsusc.2005.11.011.

Ghazy, M., Askalany, A.A., Harby, K., Ahmed, M.S., 2016. Adsorption isotherms and kinetics of HFC-404A onto bituminous based granular activated carbon for storage and cooling applications. Appl. Therm. Eng. 105, 639–645. doi:10.1016/j.applthermaleng.2016.03.057.

Ghazy, M., Askalany, A.A., Saha, B.B., 2020. Maxsorb III/HFC404A as an adsorption pair for renewable energy driven systems. Int. J. Refrig. doi:10.1016/j.ijrefrig.2020.06.017.

Gordeeva, L., Aristov, Y., 2014. Dynamic study of methanol adsorption on activated carbon ACM-35.4 for enhancing the specific cooling power of adsorptive chillers. Appl. Energy 117, 127–133. doi:10.1016/j.apenergy.2013.11.073.

Habib, K., Saha, B.B., Rahman, K.A., Chakraborty, A., Koyama, S., Ng, K.C., 2010. Experimental study on adsorption kinetics of activated carbon/R134a and activated carbon/R507A pairs. Int. J. Refrig. 33, 706–713. doi:10.1016/j.ijrefrig.2010.01.006.

Han, B., Chakraborty, A., 2019. Water adsorption studies on synthesized alkali-ions doped Al-fumarate MOFs and Al-fumarate + zeolite composites for higher water uptakes and faster kinetics. Microporous Mesoporous Mater. 288. doi:10.1016/j.micromeso.2019.109590.

Haykiri-Acma, H., Yaman, S., Kucukbayrak, S., 2006. Effect of heating rate on the pyrolysis yields of rapeseed. Renew. Energy 31, 803–810. doi:10.1016/j.renene.2005.03.013.

Hu, P., Yao, J.J., Chen, Z.S., 2009. Analysis for composite zeolite/foam aluminum-water mass recovery adsorption refrigeration system driven by engine exhaust heat. Energy Convers. Manag. 50, 255–261. doi:10.1016/j.enconman.2008.09.022.

Ismail, A.bin, Loh, W.S., Thu, K., Ng, K.C., 2013. A study on the kinetics of propane-activated carbon: theory and experiments. Appl. Mech. Mater. 388, 76–82. doi:10.4028/www.scientific.net/AMM.388.76.

Jribi, S., Miyazaki, T., Saha, B.B., Pal, A., Younes, M.M., Koyama, S., Maalej, A., 2017. Equilibrium and kinetics of CO_2 adsorption onto activated carbon. Int. J. Heat Mass Transf. 108, 1941–1946. doi:10.1016/j.ijheatmasstransfer.2016.12.114.

Jribi, S., Saha, B.B., Koyama, S., Bentaher, H., 2014. Modeling and simulation of an activated carbon-CO_2 four bed based adsorption cooling system. Energy Convers. Manag. 78, 985–991. doi:10.1016/j.enconman.2013.06.061.

Lenzen, D., Bendix, P., Reinsch, H., Fröhlich, D., Kummer, H., Möllers, M., Hügenell, P.P.C., Gläser, R., Henninger, S., Stock, N., 2018. Scalable green synthesis and full-scale test of the metal–organic framework CAU-10-H for use in adsorption-driven chillers. Adv. Mater. 30. doi:10.1002/adma.201705869.

Lu, Z., 2019. Experimental and simulation analysis of the combined adsorption system driven by 80–140 °C heat source. Energy Convers. Manag. 184, 726–734. doi:10.1016/j.enconman.2019.01.048.

Mohammed, R.H., Mesalhy, O., Elsayed, M.L., Chow, L.C., 2019a. Performance enhancement of adsorption beds with silica-gel particles packed in aluminum foams. Int. J. Refrig. 104, 201–212. doi:10.1016/j.ijrefrig.2019.03.013.

Mohammed, R.H., Mesalhy, O., Elsayed, M.L., Chow, L.C., 2019b. Assessment of numerical models in the evaluation of adsorption cooling system performance. Int. J. Refrig. 99, 166–175. doi:10.1016/j.ijrefrig.2018.12.017.

Mohammed, R.H., Mesalhy, O., Elsayed, M.L., Chow, L.C., 2018a. Experimental and numerical investigation of a new silica-gel/water packed bed for adsorption cooling applications. In: Proceedings of the Thermal Fluids Engineering Summer Conference doi:10.1615/TFEC2018.prm.021615.

Mohammed, R.H., Mesalhy, O., Elsayed, M.L., Chow, L.C., 2018b. Performance evaluation of a new modular packed bed for adsorption cooling systems. Appl. Therm. Eng. 136, 293–300. doi:10.1016/j.applthermaleng.2018.02.103.

Mohammed, R.H., Mesalhy, O., Elsayed, M.L., Su, M., Chow, C., 2018c. Revisiting the adsorption equilibrium equations of silica-gel/water for adsorption cooling applications. Int. J. Refrig. 86, 40–47. doi:10.1016/j.ijrefrig.2017.10.038.

Pal, A., Uddin, K., Thu, K., Saha, B.B., 2019. Activated carbon and graphene nanoplatelets based novel composite for performance enhancement of ad-

sorption cooling cycle. Energy Convers. Manag. 180, 134–148. doi:10.1016/j.enconman.2018.10.092.

Rezk, A., AL-Dadah, R., Mahmoud, S., Elsayed, A., 2013. Investigation of Ethanol/metal organic frameworks for low temperature adsorption cooling applications. Appl. Energy 112, 1025–1031. doi:10.1016/j.apenergy.2013.06.041.

Rupa, M.J., Pal, A., Saha, B.B., 2020. Activated carbon-graphene nanoplatelets based green cooling system: Adsorption kinetics, heat of adsorption, and thermodynamic performance. Energy 193. doi:10.1016/j.energy.2019.116774.

Ruthven, D.M., 2008. Fundamentals of adsorption equilibrium and kinetics in microporous solids. In: Molecular Sieves - Science and Technology. Springer, pp. 1–43. doi:10.1007/3829_007.

Saha, B.B., Habib, K., El-Sharkawy, I.I., Koyama, S., 2009. Adsorption characteristics and heat of adsorption measurements of R-134a on activated carbon. Int. J. Refrig. 32, 1563–1569. doi:10.1016/j.ijrefrig.2009.03.010.

Salas-Enríquez, B.G., Torres-Huerta, A.M., Conde-Barajas, E., Domínguez-Crespo, M.A., Díaz-García, L., de la Negrete-Rodríguez, M.L.X., 2016. Activated carbon production from the Guadua amplexifolia using a combination of physical and chemical activation. J. Therm. Anal. Calorim. 124, 1383–1398. doi:10.1007/s10973-016-5238-8.

Schneider, P., 1995. Adsorption isotherms of microporous-mesoporous solids revisited. Appl. Catal. A, Gen. doi:10.1016/0926-860X(95)00110-7.

Shabir, F., Sultan, M., Miyazaki, T., Saha, B.B., Askalany, A., Ali, I., Zhou, Y., Ahmad, R., Shamshiri, R.R., 2020. Recent updates on the adsorption capacities of adsorbent-adsorbate pairs for heat transformation applications. Renew. Sustain. Energy Rev. doi:10.1016/j.rser.2019.109630.

Sur, A., Sah, R.P., Pandya, S., 2020. Milk storage system for remote areas using solar thermal energy and adsorption cooling. Mater. Today Proc 28, 1764–1770. doi:10.1016/j.matpr.2020.05.170.

Thu, K., Kim, Y.D., Ismil, A.Bin, Saha, B.B., Ng, K.C., 2014. Adsorption characteristics of methane on Maxsorb III by gravimetric method. Appl. Therm. Eng. 72, 200–205. doi:10.1016/j.applthermaleng.2014.04.076.

Thu, K., Takeda, N., Miyazaki, T., Saha, B.B., Koyama, S., Maruyama, T., Maeda, S., Kawamata, T., 2019. Experimental investigation on the performance of an adsorption system using Maxsorb III + ethanol pair. Int. J. Refrig. 105, 148–157. doi:10.1016/j.ijrefrig.2018.06.009.

Tóth, J., 1995. Uniform interpretation of gas/solid adsorption. Adv. Colloid Interface Sci. doi:10.1016/0001-8686(94)00226-3.

Xia, X., Liu, Z., Li, S., 2020. Adsorption characteristics and cooling/heating performance of COF-5. Appl. Therm. Eng. 176. doi:10.1016/j.applthermaleng.2020.115442.

Xu, Z., Yin, Y., Shao, J., Liu, Y., Zhang, L., Cui, Q., Wang, H., 2020. Study on heat transfer and cooling performance of copper foams cured MIL-101 adsorption unit tube. Energy 191. doi:10.1016/j.energy.2019.116302.